АСТРОФИЗИКА

ТОМ 68 ФЕВРАЛЬ, 2025 ВЫПУСК 1

DOI: 10.54503/0571-7132-2025.68.1-117

LGV ANALYSIS OF HYDROPEROXY RADICAL (HO_2): SPECTRAL LINES FOR ITS DETECTION IN A COSMIC OBJECT

S.CHANDRA

Received 17 October 2024
Accepted 14 February 2025

Knowing rotational and centrifugal distortion constants in conjunction with electric dipole moment for HO_2 radical, we have calculated energies for rotational levels (without fine-structure splitting), and probabilities for radiative transitions between the levels. The radiative transition probabilities in conjunction with the scaled values for rate coefficients for collisional transitions between the levels, the Large Velocity Gradient (LVG) analysis for HO_2 is performed. Two observed lines, 2_{02}-1_{01} and 4_{04}-3_{03} of HO2 are found to show MASER action. Seven lines 1_{10}-1_{11}, $2_{1.1}$-$2_{1.2}$, $3_{1.2}$-$3_{1.3}$, $4_{1.3}$-$4_{1.4}$, $5_{1.4}$-$5_{1.5}$, $6_{1.5}$-$6_{0.6}$ and $7_{1.6}$-$7_{0.7}$ are found to show anomalous absorption and five more lines, $7_{1.6}$-$7_{1.7}$, $1_{1.0}$-$1_{0.1}$, $2_{2.1}$-$3_{1.2}$, $4_{2.3}$-$3_{1.2}$ and $4_{4.1}$-$3_{3.0}$ are found to show MASER action. These 14 lines are analyzed here and they may play key role in the identification of HO_2 in a cosmic object.

Keywords: *ISM: molecules: radiative transitions: collisional transitions: HO_2: LVG analysis*

1. *Introduction*. The hydroperoxy radical HO_2 is a short-lived species which plays important role as a transient intermediate in a large number of chemical reactions. The HO_2 radical is found in the boundary layer of coastal Antarctica [1], upper troposphere [2,3], middle atmosphere [4], North Atlantic free troposphere [5], upper stratosphere [6]. It is considered a potential tracer of interstellar molecular oxygen [7]. Widicus Weaver et al. [8] have discussed if HO_2^+ is detectable in interstellar medium. It has important role, for example, in the chemistry of atmospheric ozone cycle and in the formation of hydrogen peroxide H_2O_2, found in the interstellar medium and on the martian surface, through the reaction:

$$HO_2 + HO_2 \rightarrow H_2O_2 + O_2 .$$

The formation of HO_2 is discussed through the series of reactions:

$$HO_2 + h\nu \rightarrow OH + H , \quad OH + CO \rightarrow H + CO_2 ,$$

$$H + O_2 + CO_2 \rightarrow HO_2 + CO_2 .$$

The contributing molecules CO, O_2 and H_2O are abundant in the molecular regions. The HO_2 is analyzed in laboratories from time to time [9-11]. The

rotational and centrifugal distortion constants derive by Charo and de Lucia [11] in I^r representation with A-reduction of Watson Hamiltonian are given in Table 1. The planar radical HO_2 has electric dipole moment with components $\mu_a = 1.41$ Debye and $\mu_b = 1.54$ Debye [12]. The HO_2 is detected towards ρ Ophiuchi A by Parise et al. [13] through the fine-structure of two rotational transitions 2_{02}-1_{01} and 4_{04}-3_{03}. In order to find other potential lines of HO_2, which may help in its detection, we have gone for the Large Velocity Gradient (LVG) analysis.

Using the rotational and centrifugal distortion constants in conjunction with electric dipole moment, we have calculated energies for 100 rotational levels (without fine-structure splitting), and probabilities for radiative transitions between the levels. The radiative transition probabilities in conjunction with the scaled values for rate coefficients for collisional transitions between the levels, the LVG analysis is performed.

In section 2, we have discussed the optimization of HO_2, in section 3, we have discussed the molecular symmetries. Section 4 is devoted for the LVG analysis. Results and discussion is given in section 5, and the conclusion is given in section 6.

2. *Optimization of HO_2.* With the help of GAUSSIAN, we have optimized the radical HO_2 where we have employed the method B3LYP and basis sets, aug-cc-pVDz, aug-cc-pVTz and aug-cc-pVQz, separately. The rotational and centrifugal distortion constants, obtained from optimization are also given in Table 1. The

Table 1

ROTATIONAL AND CENTRIFUGAL DISTORTION CONSTANTS IN MHz

Constant	Experimental	aug-cc-pVDz	aug-cc-pVTz	aug-cc-pVQz
A	610273.223	594875.9274	620241.5483	623206.4161
B	33517.816	31752.3379	33712.1785	33842.9333
C	31667.654	30143.3921	31974.2712	32099.7703
Δ_N	0.11693	0.113154308	0.109667331	0.109728139
Δ_{NK}	3.44552	-0.941687383	3.259860266	3.286684145
Δ_K	123.572	141.266600505	96.768558195	97.857592968
δ_N	0.00613	0.007082461	0.005402967	0.005401713
δ_K	2.017	0.798954199	1.655319807	1.668854530
H_{NK}	$2.29 \cdot 10^{-5}$			
H_{KN}	$1.051 \cdot 10^{-3}$			
H_K	$9.69 \cdot 10^{-2}$			

coordinates of its constituent atoms obtained from GAUSSIAN using B3LPY/aug-cc-pVTz are shown in the following table:

STRUCTURE OF HO_2 RADICAL

Atom	Coordinates (Å)		
	x	*y*	*z*
H	-0.869263	-0.886030	0.000000
O	0.055377	-0.609725	0.000000
O	0.055377	0.718382	0.000000

3. *Molecular symmetries*. The selection rules for the rotational quantum number J for the non-radiative (collisional) transitions are:

$$\Delta J = 0, \pm 1, \pm 2, \pm 3, ...$$

Let us consider the collisional transitions only for k_a, k_c levels. Each of the pseudo quantum number, k_a and k_c can independently assume even (*e*) and odd (*o*) positive integer values, including zero. When the electric dipole moment is along the *a*-axis of inertia, the following collisional transitions for $k_a k_c$ are not allowed.

$$(e,o) \leftrightarrow (o,e), \qquad (e,e) \leftrightarrow (o,o) \tag{1}$$

$$(e,o) \leftrightarrow (o,o), \qquad (e,e) \leftrightarrow (o,e). \tag{2}$$

These rules divide the rotational levels into the ortho and para species. The allowed collisional transitions are:

$$(o,e) \leftrightarrow (o,o) \quad (o,o) \leftrightarrow (o,o) \quad (o,e) \leftrightarrow (o,e) \quad (\text{Group I}) \tag{3}$$

$$(e,o) \leftrightarrow (e,e) \quad (e,o) \leftrightarrow (e,o) \quad (e,e) \leftrightarrow (e,e) \quad (\text{Group II}) \tag{4}$$

The above can be verified from the papers published for *a*-type molecules.When the electric dipole moment is along the *b*-axis of inertia, the following collisional transitions for k_a, k_c are not allowed.

$$(e,o) \leftrightarrow (e,e) \qquad (o,e) \leftrightarrow (o,o) \tag{5}$$

$$(e,o) \leftrightarrow (o,o) \qquad (o,e) \leftrightarrow (e,e) \tag{6}$$

These rules divide the rotational levels into the ortho and para species. The allowed collisional transitions are:

$$(e,o) \leftrightarrow (o,e) \quad (e,o) \leftrightarrow (e,o) \quad (o,e) \leftrightarrow (o,e) \quad (\text{Group III}) \tag{7}$$

$$(e,e) \leftrightarrow (o,o) \quad (e,e) \leftrightarrow (e,e) \quad (o,o) \leftrightarrow (o,o) \quad (\text{Group IV}). \tag{8}$$

The above can be verified from the papers published for *b*-type molecules.

The electric dipole moment of HO_2 has components: $\mu_a = 1.41$ Debye and $\mu_b = 1.54$ Debye. We have considered both *a* and *b* type transitions together. Thus, the transitions (5) are allowed due to a component of dipole moment, and the transitions (1) are allowed due to b component of dipole moment. However, still

the transitions (6) as well as the transitions (2) are not allowed. Considered 100 levels given in Table 2, may be classified into 4 groups, I, II, III and IV, as the following (here, the digits are the Nos. of the levels):

Group I:

1, 2, 3, 4, 7, 12, 15, 18, 21, 24, 25, 26, 27, 29, 31, 32, 33, 34, 37, 38, 39, 41, 42, 44, 45, 46, 49, 50, 51, 58, 59, 60, 67, 68, 69, 73, 74, 78, 81, 82, 87, 88, 89, 94, 95, 96, 97, 98, 99, 100.

Group II:

5, 6, 8, 9, 10, 11, 13, 14, 16, 17, 19, 20, 22, 23, 28, 30, 35, 36, 40, 43, 47, 48, 52, 53, 54, 55, 56, 57, 61, 62, 63, 64, 65, 66, 70, 71, 72, 75, 76, 77, 79, 80, 83, 84, 85, 86, 90, 91, 92, 93.

Group III:

2, 4, 6, 8, 11, 12, 13, 17, 18, 19, 23, 24, 27, 28, 29, 31, 34, 36, 38, 40, 42, 44, 45, 48, 51, 53, 54, 56, 58, 60, 62, 64, 66, 68, 71, 72, 73, 76, 78, 80, 82, 84, 85, 88, 90, 92, 94, 96, 98, 100.

Table 2

ENERGY LEVELS AND THEIR ENERGIES IN cm^{-1}

No.	Level	Energy	No.	Level	Energy	No.	Level	Energy	No.	Level	Energy
1	$0_{0.0}$	0.0000	26	$3_{2.2}$	89.9894	51	$9_{2.7}$	174.7055	76	$8_{3.6}$	251.1057
2	$1_{0.1}$	2.1728	27	$3_{2.1}$	89.9901	52	$3_{3.1}$	185.9971	77	$8_{3.5}$	251.1058
3	$2_{0.2}$	6.5183	28	$8_{1.8}$	96.3350	53	$3_{3.0}$	185.9971	78	$15_{0.15}$	260.1737
4	$3_{0.3}$	13.0358	29	$9_{0.9}$	97.6987	54	$12_{1.12}$	186.1981	79	$9_{3.7}$	270.6340
5	$1_{1.1}$	21.3938	30	$8_{1.7}$	98.5433	55	$12_{1.11}$	190.9765	80	$9_{3.6}$	270.6342
6	$1_{1.0}$	21.4552	31	$4_{2.3}$	98.6760	56	$4_{3.2}$	194.6795	81	$13_{2.12}$	274.4470
7	$4_{0.4}$	21.7247	32	$4_{2.2}$	98.6782	57	$4_{3.1}$	194.6795	82	$13_{2.11}$	274.6446
8	$2_{1.2}$	25.6775	33	$5_{2.4}$	109.5334	58	$10_{2.9}$	196.3579	83	$15_{1.15}$	275.9893
9	$2_{1.1}$	25.8617	34	$5_{2.3}$	109.5385	59	$10_{2.8}$	196.4297	84	$15_{1.14}$	283.3302
10	$3_{1.3}$	32.1028	35	$9_{1.9}$	115.5975	60	$13_{0.13}$	197.4025	85	$10_{3.8}$	292.3296
11	$3_{1.2}$	32.4711	36	$9_{1.8}$	118.3571	61	$5_{3.3}$	205.5320	86	$10_{3.7}$	292.3300
12	$5_{0.5}$	32.5841	37	$10_{0.10}$	119.3876	62	$5_{3.2}$	205.5320	87	$16_{0.16}$	294.7781
13	$4_{1.4}$	40.6692	38	$6_{2.5}$	122.5610	63	$13_{1.13}$	213.9983	88	$14_{2.13}$	304.8014
14	$4_{1.3}$	41.2831	39	$6_{2.4}$	122.5712	64	$6_{3.4}$	218.5542	89	$14_{2.12}$	305.0646
15	$6_{0.6}$	45.6128	40	$10_{1.10}$	136.9963	65	$6_{3.3}$	218.5542	90	$16_{1.16}$	310.1767
16	$5_{1.5}$	51.3764	41	$7_{2.6}$	137.7582	66	$13_{1.12}$	219.5707	91	$11_{3.9}$	316.1920
17	$5_{1.4}$	52.2970	42	$7_{2.5}$	137.7765	67	$11_{2.10}$	220.2237	92	$11_{3.8}$	316.1926
18	$7_{0.7}$	60.8092	43	$10_{1.9}$	140.3682	68	$11_{2.9}$	220.3275	93	$16_{1.15}$	318.4916
19	$6_{1.6}$	64.2235	44	$11_{0.11}$	143.2364	69	$14_{0.14}$	227.7141	94	$4_{4.1}$	328.7455
20	$6_{1.5}$	65.5123	45	$8_{2.7}$	155.1240	70	$7_{3.5}$	233.7456	95	$4_{4.0}$	328.7455
21	$8_{0.8}$	78.1718	46	$8_{2.6}$	155.1545	71	$7_{3.4}$	233.7457	96	$17_{0.17}$	331.5234
22	$7_{1.7}$	79.2101	47	$11_{1.11}$	160.5303	72	$14_{1.14}$	243.9292	97	$15_{2.14}$	337.3156
23	$7_{1.6}$	80.9280	48	$11_{1.10}$	164.5751	73	$12_{2.11}$	246.2539	98	$15_{2.13}$	337.6593
24	$2_{2.1}$	83.4740	49	$12_{0.12}$	169.2422	74	$12_{2.10}$	246.3990	99	$5_{4.2}$	339.5898
25	$2_{2.0}$	83.4742	50	$9_{2.8}$	174.6576	75	$14_{1.13}$	250.3559	100	$5_{4.1}$	339.5898

Group IV:

1, 3, 5, 7, 9, 10, 14, 15, 16, 20, 21, 22, 25, 26, 30, 32, 33, 35, 37, 39, 41, 43, 46, 47, 49, 50, 52, 55, 57, 59, 61, 63, 65, 67, 69, 70, 74, 75, 77, 79, 81, 83, 86, 87, 89, 91, 93, 95, 97, 99.

The radiative as well as collisional transitions are within each group, separately. The radiative transitions follow the selection rules whereas the collisional transitions do not follow any selection rules. However, they are confined within a group, individually. Thus, a level is not connected to all other 99 levels.

4. *LVG analysis*. For investigation, suppose, z lower rotational levels of a given molecule are considered. These levels are connected through radiative and non-radiative (collisional) transitions, as the pumping may be collisional as well as radiative. In the steady state, for these z levels, a set of statistical equilibrium equations coupled with the equations of radiative transfer is expressed as (Large Velocity Gradient LVG analysis)

$$n_i \sum_{\substack{j=1 \\ j\neq i}}^{z} P_{ij} = \sum_{\substack{j=1 \\ j\neq i}}^{z} n_j P_{ji}\,, \quad i = 1, 2, ..., z, \tag{9}$$

where n denotes the population density of energy level and the parameter P is expressed as the following.

$$P_{ij} = \begin{cases} A_{ij}\,\beta_{ij} + B_{ij}\,\beta_{ij}\,I_{v,bg} + n_{H_2} C_{ij}\,, & i > j\,, \\ B_{ij} I_{v,bg}\,\beta_{ij} + n_{H_2} C_{ij}\,, & i < j\,. \end{cases} \tag{10}$$

Here, understanding is that for the optically allowed transitions, both the A and B Einstein coefficients are non-zero, whereas for the optically forbidden transitions, the A and B both are zero. To account for the LVG analysis, the Einstein A and B coefficients are multiplied by the escape probability β. Further, we have

$$I_{v,bg} = \frac{8\pi h v^3}{c^2} \frac{1}{\exp\left(hv/kT_{bg}\right) - 1}, \tag{11}$$

where T_{bg} is background temperature 2.73 K, C is the rate coefficient for collisional transition and n_{H_2} is density of molecular hydrogen (colliding partner) in the region. The escape probability β for transition is

$$\beta_{lu} = \beta_{ul} = \frac{1 - \exp\left(-\tau_v\right)}{\tau_v}, \tag{12}$$

where optical thickness τ_v is expressed as

$$\tau_v = h\gamma\left[B_{lu} n_l - B_{ul} n_u\right], \tag{13}$$

where $\gamma = N_{mol}/\Delta v_r$; N_{mol} is the column density of the molecule in the object and Δv_r is the radial velocity-shift in the object.

4.1. *Radiative transitions*. The electric dipole moment of HO_2 has components $\mu_a = 1.41$ Debye and $\mu_b = 1.54$. Using the electric dipole moment components, Einstein *A*-coefficients for both *a* and *b* type rotational transitions are calculated. The Einstein *A*-coefficient is related to the Einstein *B*-coefficients, for a radiative transition between upper and lower levels *u* and *l*, respectively, through the relations:

$$A_{ul} = \frac{8\pi h\nu^3}{c^3} B_{ul}, \quad \text{and} \quad B_{lu} = \frac{g_u}{g_l} B_{ul}, \tag{14}$$

where g_u and g_l denote the statistical weights for the upper and lower levels, respectively. The 100 rotational levels are connected through 463 radiative transitions. Before calculating Einstein *A*-coefficients, we looked for the JPL database. There we could find information for 399 out of 463 transitions. Therefore, we have decided for calculations of Einstein *A*-coefficients

4.2. *Collisional transitions*. Though the collisional transitions between the levels of each group do not follow any kind of selection rules, but their computation is very difficult task [14-16]. Using a scaling law, discussed by Sharma et al. [17,18] the collisional rate coefficients are calculated.

4.3. *Radiative life-time*. For a rotational level *j*, the radiative life-time T_j is defined as

$$T_j = 1 \Big/ \sum_i A_{ji}, \tag{15}$$

where A_{ji} denotes the Einstein *A*-coefficient for radiative transition from the level *j* to a lower level *i* and the summation is taken for all the downward radiative transitions. The radiative life-time of upper level, in general, is smaller than that of the lower level. For some transitions, the reverse is the case.

5. *Results and discussion*. For the assigned values of kinetic temperature *T*, molecular hydrogen density n_{H_2}, and γ, equation (9) is a homogeneous set of equations, and therefore cannot have unique solution. In order to make the set of equations inhomogeneous, one of the equations in the set is replaced by the following equation.

$$\sum_{i=1}^{z} n_i = n_{total}. \tag{16}$$

The value of n_{total} can be taken as 1, as we deal with the ratio of population densities of levels. We have solved a set of statistical equilibrium equations coupled with the equations of radiative transfer through iterative procedure, where the initial population densities are taken as the thermal population densities corresponding to the kinetic temperature in the region.

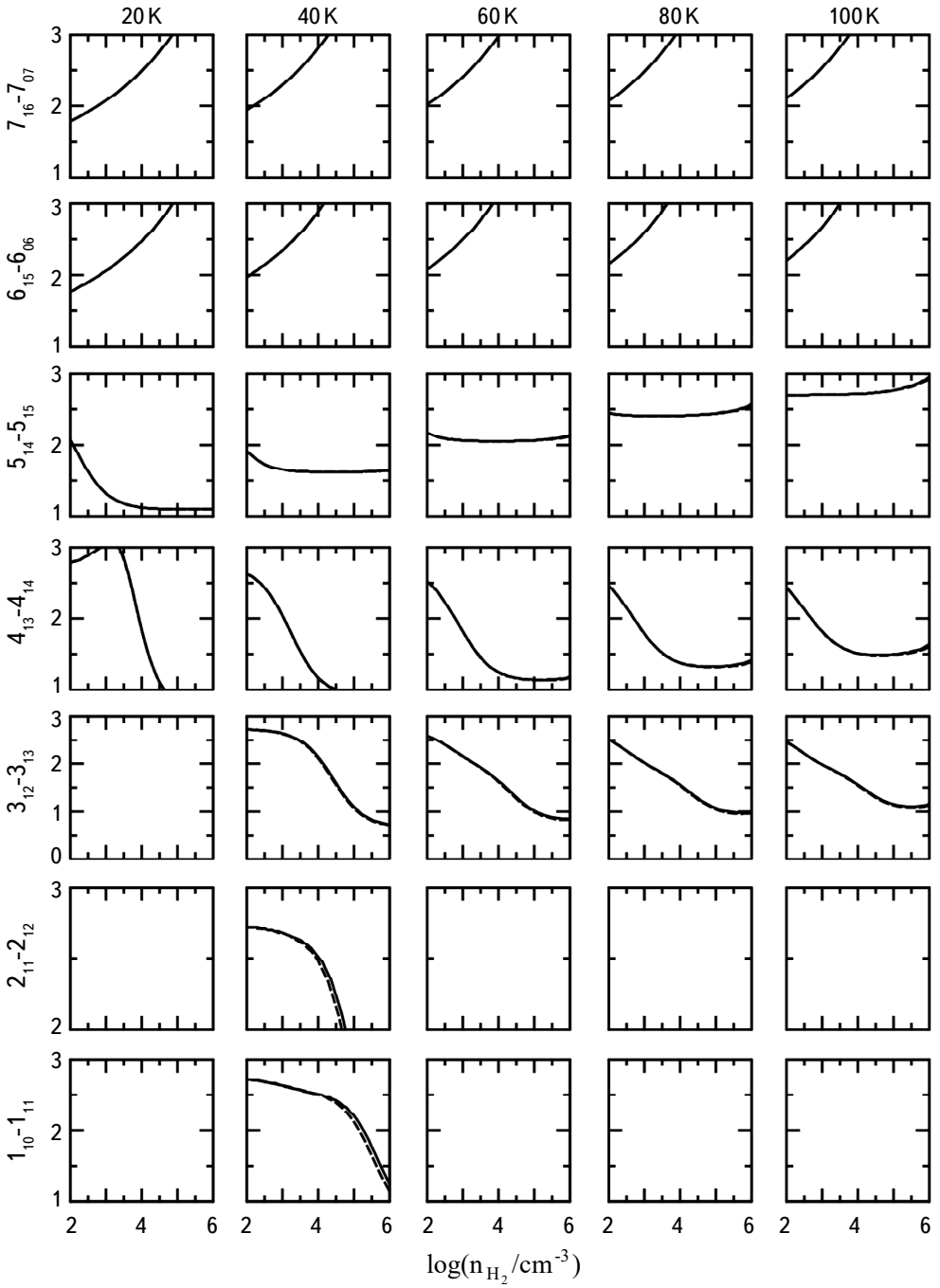

Fig.1. Variation of excitation temperatures T_{ex} (K) versus molecular hydrogen density n_{H_2} for kinetic temperatures of 20, 40, 60, 80 and 100 K (written on the top) for seven transitions, 1_{10}-1_{11}, 2_{11}-2_{12}, 3_{12}-3_{13}, 4_{13}-4_{14}, 5_{14}-5_{15}, 6_{15}-6_{06}, 7_{16}-7_{07} (written on the left) of HO_2. Solid line is for $\gamma = 10^{-5}$ cm^{-3} (km/s)$^{-1}$ pc, and the dotted line for $\gamma = 10^{-6}$ cm^{-3} (km/s)$^{-1}$ pc.

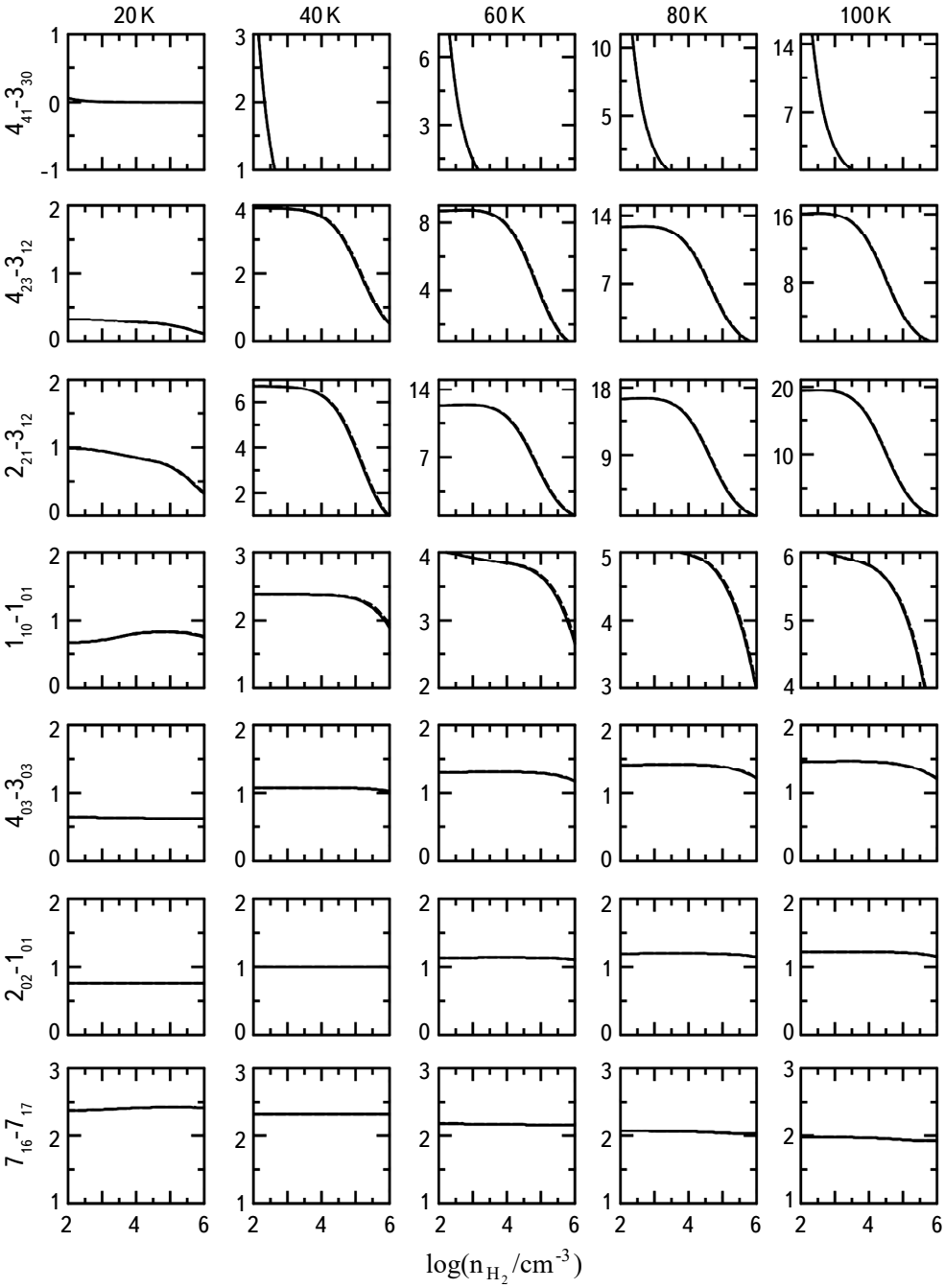

Fig.2. Variation of $n_u g_l / n_l g_u$ versus molecular hydrogen density n_{H_2} for kinetic temperatures of 20, 40, 60, 80 and 100 K (written on the top) for seven transitions, 7_{16}-7_{17}, 2_{02}-1_{01}, 4_{03}-3_{03}, 1_{10}-1_{01}, 2_{21}-3_{12}, 4_{23}-3_{12} and 4_{41}-3_{30} (written on the left) of HO_2. Solid line is for $\gamma = 10^{-5}$ cm^{-3} (km/s)$^{-1}$ pc, and the dotted line for $\gamma = 10^{-6}$ cm^{-3} (km/s)$^{-1}$ pc.

The excitation temperature T_{ex} for a line between an upper level *u* and a lower level *l* is expressed as

$$T_{ex} = -\frac{\Delta E_{ul}}{k \ln\left(n_u g_l / n_l g_u\right)},$$

where ΔE_{ul} is the energy difference between the two levels. For low density in a region, the collisional rates are very small as compared to the radiative transition rates, and the population densities of levels are governed by the radiative transitions. Therefore, the excitation temperature tends to the CMB temperature of 2.73 K.

Seven lines 1_{10}-1_{11}, $2_{1.1}$-$2_{1.2}$, $3_{1.2}$-$3_{1.3}$, $4_{1.3}$-$4_{1.4}$, $5_{1.4}$-$5_{1.5}$, $6_{1.5}$-$6_{0.6}$ and $7_{1.6}$-$7_{0.7}$ are found to show anomalous absorption. Variation of excitation temperatures T_{ex} (K) versus molecular hydrogen density n_{H_2} for kinetic temperatures of 20, 40, 60, 80 and 100 K for these lines are shown in Fig.1. For first two lines, the graphs are shown for 40 K only, where the variation is smooth.

For the MASER action, population inversion ($n_u g_l / n_l g_u > 1$) between the upper level *u* and lower level *l* is required.

$$\frac{n_u g_l}{n_l g_u} > 1.$$

Table 3

FREQUENCY ν, A - COEFFICIENT A_{ul}, ENERGY E_u OF UPPER LEVEL RADIATIVE LIFE-TIME t_u OF UPPER LEVEL AND t_l OF LOWER LEVEL FOR TRANSITIONS

Transition	ν (MHz)	A_{ul} (s^{-1})	E_u (cm^{-1})	t_u (s)	t_l (s)
MASER transitions					
$7_{1.6}$-$7_{1.7}$	51538.846	5.658E-08	80.928	2.49E+02	1.16E+02
$2_{0.2}$-$1_{0.1}$	130362.828	2.051E-05	6.518	4.88E+04	4.68E+05
$4_{0.4}$-$3_{0.3}$	260668.262	1.822E-04	21.725	5.49E+03	1.35E+04
$1_{1.0}$-$1_{0.1}$	578471.150	2.672E-03	21.455	3.74E+02	4.68E+05
$2_{2.1}$-$3_{1.2}$	1530086.220	3.316E-03	83.474	1.24E+01	3.58E+02
$4_{2.3}$-$3_{1.2}$	1986146.090	4.508E-02	98.676	1.21E+01	3.58E+02
$4_{4.1}$-$3_{3.0}$	4282451.060	8.429E-01	328.745	9.63E-01	2.64E+00
Anomalous absorption transitions					
$1_{1.0}$-$1_{1.1}$	1842.045	7.232E-11	21.455	3.74E+02	3.52E+02
$2_{1.1}$-$2_{1.2}$	5525.841	6.508E-10	25.862	3.69E+02	3.10E+02
$3_{1.2}$-$3_{1.3}$	11050.792	2.602E-09	32.471	3.58E+02	2.62E+02
$4_{1.3}$-$4_{1.4}$	18415.991	7.227E-09	41.283	3.39E+02	2.16E+02
$5_{1.4}$-$5_{1.5}$	27620.197	1.625E-08	52.297	3.14E+02	1.76E+02
$6_{1.5}$-$6_{0.6}$	596985.070	2.890E-03	65.512	2.83E+02	1.57E+03
$7_{1.6}$-$7_{0.7}$	603563.850	2.970E-03	80.928	2.49E+02	9.78E+02

Seven lines 7_{16}-7_{17}, 2_{02}-1_{01}, 4_{03}-3_{03}, 1_{10}-1_{01}, 2_{21}-3_{12}, 4_{23}-3_{12} and 4_{41}-3_{30} are found to show MASER action. The variation of nu gl/nl gu versus molecular hydrogen density n_{H_2} for kinetic temperatures of 20, 40, 60, 80 and 100 K for these lines are shown in Fig.2.

Information about these 14 anomalous absorption and MASER lines are given in Table 3, where we have given the frequency, Einstein *A*-coefficient, energy of upper level of transition, and radiative life-times of upper and lower levels of the transition.

6. *Conclusion*. For known rotational and centrifugal distortion constants, and electric dipole moment for HO_2 radical, energies of 100 rotational levels are calculated. As both the *a* and *b* components of electric dipole moment are considered together, the levels are classified in four groups. The radiative and collisional transitions between the rotational levels are considered in each group, separately. The LVG analysis is performed, where collisional rate coefficients are calculated using a scaling law. Seven lines are found to show anomalous absorption and seven lines are found to shows MASER action. Two observed lines of HO_2 are among the lines showing the MASER action.

Acknowledgments. Thanks are due to the learned reviewer for encouraging and constructive comments. The author is grateful to Hon'ble Dr. Ashok K.Chauhan, Founder President, Hon'ble Dr. Atul Chauhan, Chancellor, and Hon'ble Prof. Dr. Balvinder Shukla, Vice Chancellor, Amity University, Noida for valuable support and encouragements.

Amity Centre for Astronomy & Astrophysics, Amity Institute of Applied Sciences, Amity University Uttar Pradesh,
India, e-mail: schandra2@amity.edu

LGV-АНАЛИЗ ГИДРОПЕРОКСИРАДИКАЛА (HO_2): СПЕКТРАЛЬНЫЕ ЛИНИИ ДЛЯ ЕГО ОБНАРУЖЕНИЯ В КОСМИЧЕСКИХ ОБЪЕКТАХ

С.ЧАНДРА

С помощью известных вращательных и центробежных констант аберрации, в сочетании с электрическим дипольным моментом для радикала HO_2, были вычислены энергия вращательных уровней (без расщепления тонкой структуры) и вероятности радиационных переходов между уровнями. Для HO_2

был проведен анализ LVG с использованием вероятностей радиационных переходов в сочетании с масштабированными значениями коэффициентов скорости столкновительных переходов между уровнями. Показано, что две наблюдаемые линии, 2_{02}-1_{01} и 4_{04}-3_{03} HO_2, являются мазерными. Кроме них обнаружено еще пять мазерных линий - $7_{1.6}$-$7_{1.7}$, $1_{1.0}$-$1_{0.1}$, $2_{2.1}$-$3_{1.2}$, $4_{2.3}$-$3_{1.2}$ и $4_{4.1}$-$3_{3.0}$. Семь линий, 1_{10}-1_{11}, $2_{1.1}$-$2_{1.2}$, $3_{1.2}$-$3_{1.3}$, $4_{1.3}$-$4_{1.4}$, $5_{1.4}$-$5_{1.5}$, $6_{1.5}$-$6_{0.6}$ и $7_{1.6}$-$7_{0.7}$, показывают аномальное поглощение. Эти 14 линий могут играть ключевую роль в идентификации HO_2 в космических объектах.

Ключевые слова: *ISM: молекулы: радиационные переходы: столкновительные переходы: HO_2: анализ LVG*

REFERENCES

1. *W.J.Bloss*, *J.D.Lee*, *D.E.Heard et al.*, Atmos. Chem. Phys. Discuss., **7**, 2893, 2007.
2. *L.Jaegle*, *D.J.Jacob et al.*, Geophys. Res. Lett., **24**, 3181, 1997.
3. *R.M.Stimpfle*, *P.O.Wennberg*, *L.B.Lapson et al.*, Geophys. Res. Lett., **17**, 1905, 1990.
4. *S.Wang*, *Q.Zhang et al.*, Geophys. Res. Lett., **42**, 10, 2015.
5. *W.H.Brune*, *D.Tan et al.*, Geophys. Res. Lett., **26**, 3077, 1999.
6. *K.W.Jucks*, *D.G.Johnson*, *K.V.Chance et al.*, Geophys. Res. Lett., **25**, 3935, 1998.
7. *R.I.Kaiser*, *G.Eich*, *A.Gabrysch et al.*, Astron. Astrophys., **346**, 340, 1999.
8. *S.L.Widicus Weaver*, *D.E.Woon*, *B.Ruscic et al.*, Astrophys. Lett., **697**, 601, 2009.
9. *Y.Beers*, *C.J.Howard*, J. Chem. Phys., **63**, 4212, 1975.
10. *S.Saito*, J. Mol. Spectrosc., **65**, 229, 1977.
11. *A.Charo*, *F.C. de Lucia et al.*, J. Mol. Spectrosc., **94**, 426, 1982.
12. *S.Saito*, *C.Matsumura*, J. Mol. Spectrosc., **80**, 34, 1980.
13. *B.Parise*, *P.Bergman*, *F.Du*, Astron. Astrophys., **541**, L11, 2012.
14. *M.Sharma*, *M.K.Sharma*, *U.P.Verma et al.*, Adv. Space Res., **54**, 252, 2014a.
15. *M.K.Sharma*, *M.Sharma*, *U.P.Verma et al.*, Adv. Space Res., **54**, 1963, 2014b.
16. *M.K.Sharma*, *M.Sharma*, *U.P.Verma et al.*, Adv. Space Res., **55**, 434, 2015.
17. *M.K.Sharma*, *M.Sharma*, *S.Chandra*, Astrophys. Space Sci., **362**, 168, 2017.
18. *M.K.Sharma*, *M.Sharma*, *S.Chandra*, Mol. Astrophys., **12**, 20, 2018.